Science of the Total Environment 804 (2022) 150039

Contents lists available at ScienceDirect

Science of the Total Environment

journal homepage: www.elsevier.com/locate/scitotenv

Multi-hazard susceptibility and exposure assessment of the Hindu Kush Himalaya

Jack Rusk [a,*], Amina Maharjan [b], Prakash Tiwari [c], Tzu-Hsin Karen Chen [a], Sara Shneiderman [d,e], Mark Turin [d,f], Karen C. Seto [a]

[a] Yale School of the Environment, Yale University, New Haven, CT 06511, USA
[b] International Centre for Integrated Mountain Development (ICIMOD), Khumaltar, Lalitpur 44700, Nepal
[c] Kumaun University, Nainital, Uttarakhand 263001, India
[d] Department of Anthropology, University of British Columbia, Vancouver, BC V6T 1Z1, Canada
[e] School of Public Policy & Global Affairs, University of British Columbia, Vancouver, BC V6T 1Z1, Canada
[f] Institute for Critical Indigenous Studies, University of British Columbia, Vancouver, BC V6T 1Z1, Canada

HIGHLIGHTS

- We propose a method to study multi-hazard susceptibility and exposure.
- Areas susceptible to floods, landslides, and wildfires largely overlapped.
- Population was concentrated in areas susceptible to multiple hazards.
- Landscapes favorable to human settlement are sites of multi-hazard risk.
- Multi-hazard risk is expected to increase in the HKH.

GRAPHICAL ABSTRACT

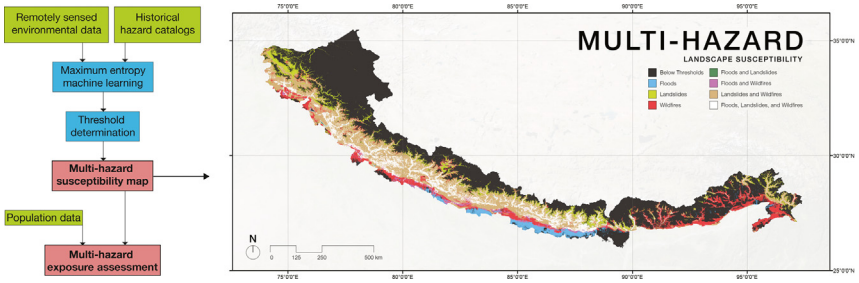

ARTICLE INFO

Article history:
Received 20 June 2021
Received in revised form 21 August 2021
Accepted 26 August 2021
Available online 30 August 2021

Editor: Fernando A.L. Pacheco

Keywords:
Hindu Kush Himalaya
Cascading and compounding hazards
Multi-hazard risk
Disaster risk reduction
Urbanization

ABSTRACT

Mountainous regions are highly hazardous, and these hazards often lead to loss of human life. The Hindu Kush Himalaya (HKH), like many mountainous regions, is the site of multiple and overlapping natural hazards, but the distribution of multi-hazard risk and the populations exposed to it are poorly understood. Here, we present high-resolution transboundary models describing susceptibility to floods, landslides, and wildfires to understand population exposure to multi-hazard risk across the HKH. These models are created from historical remotely sensed data and hazard catalogs by the maximum entropy (Maxent) machine learning technique. Our results show that human settlements in the HKH are disproportionately concentrated in areas of high multi-hazard risk. In contrast, low-hazard areas are disproportionately unpopulated. Nearly half of the population in the region lives in areas that are highly susceptible to more than one hazard. Warm low-altitude foothill areas with perennially moist soils were identified as highly susceptible to multiple hazards. This area comprises only 31% of the study region, but is home to 49% of its population. The results also show that areas susceptible to multiple hazards are also major corridors of current migration and urban expansion, suggesting that current rates and patterns of urbanization will continue to put more people at risk. This study establishes that the population in the HKH is concentrated in areas susceptible to multiple hazards and suggests that current patterns of human movement will continue to increase exposure to multi-hazards in the HKH.

* Corresponding author.
E-mail address: jack.rusk@yale.edu (J. Rusk).

https://doi.org/10.1016/j.scitotenv.2021.150039

1. Introduction

The 6th Assessment of the IPCC Report makes clear that climate change is resulting in multiple changes in many regions (IPCC, 2021). In particular, mountain areas are likely to experience *cascading* consequences of floods, landslides and other events associated with increased warming and extreme precipitation (Arias et al., 2021). The topography, geological processes, and hydrological character of mountainous regions provide water, resources, and ecosystem services to downstream areas, but also make the lives of mountain residents and their settlements vulnerable to multiple interacting natural hazards. Globally, mountain regions are hot spots for hazard mortality: over 70% of the more than 700,000 disaster-related deaths between 2005 and 2014 occurred in mountainous countries (UNISDR, 2015, cited in Klein et al., 2019). In 1992, sustainable mountain development was articulated as a global intergovernmental priority in Chapter 13 of Agenda 21 (UNCED, 1992). Agenda 21 recommends evaluating and mitigating the risks posed by hazards in mountainous areas, asserting that mitigation of multi-hazard risk is intrinsic to sustainable mountain development. Exacerbating the risks posed by these hazards, mountain populations worldwide have grown in step with the global population—increasing by more than 170 million people this century—and these mountain populations are urbanizing (Ehrlich et al., 2021).

The Hindu Kush Himalaya (HKH), the extent of which considered here is delineated in Section 2 below, is exemplary of cascading and compounding risks associated with climate change, as well as the connection between sustainable mountain development and hazard risk mitigation. The HKH is a global hazard hotspot and is among the highest places globally for mortality risk associated with hydrological and geophysical hazards (Dilley et al., 2005). The presence of multiple interacting hazards, together with lagging development and inadequate risk mitigation, have had costly and fatal consequences in the HKH. The 2015 Gorkha earthquake triggered over 24,000 landslides, a compounding multi-hazard event that destroyed over 500,000 formal and informal structures, killed almost 9000 people, and displaced 2.8 million more (Molden et al., 2016; Roback et al., 2018). In 2013, rainfall triggered simultaneous compounding landslides and flash floods in the Garhwal Himalaya, destroying over 200 buildings and leading to several fatalities (Bhambri et al., 2016). In 2003, a landslide dammed the Paree Chu stream in Himachal Pradesh; cascading from that event, the dam's rupture in 2005 caused 177 million USD in damage to downstream settlements (Gupta and Sah, 2008). In February 2021, a flood in the Chamoli District of Uttarakhand caused 70 confirmed fatalities and over 100 injuries; initially thought to be caused by a glacial lake outburst, remote sensing showed that the flood was caused by the rapid fluidization of ice from the kinetic energy of the rockfall combining with a stream below (Shrestha et al., 2021).

While these examples demonstrate that the HKH, like other mountainous regions, is vulnerable to compounding or cascading multi-hazard events, it is nonetheless common for studies to focus solely on a single hazard (Aryal et al., 2020; Bera et al., 2019; Kappes et al., 2012; Pangali Sharma et al., 2019; Vilà-Vilardell et al., 2020; Zimmermann and Keiler, 2015). While single hazard assessments yield important insights, they can also obscure interactions between hazards (Kappes et al., 2010). These interactions—in which one hazard triggers, intensifies, attenuates, or preconditions another, or when two hazards share similar triggers and may even occur simultaneously—can compound hazard risk or link hazards into cascading hazard sequences (Kappes et al., 2010; Cutter, 2018). These interactions are definitive aspects of risk in areas highly susceptible to multiple hazards, such as mountainous regions (Kappes et al., 2010; Zimmermann and Keiler, 2015).

In the Hindu Kush Himalaya, urban settlements are small in scale but patterns of urbanization have a broadly transboundary character (Aryal et al., 2018; Mukherji et al., 2018). Urbanization in the HKH is driven by complex local, regional, and international migration patterns, from seasonal movement for agricultural work between Nepal and India, to the ongoing depopulation of highland villages as people settle in urban centers, to outmigration into other parts of Asia and the Gulf states (Aryal et al., 2018; Mukherji et al., 2018). Urbanization in the region is changing patterns of susceptibility and exposure to multi-hazard risk (Rose et al., 2020; Tiwari et al., 2018). When urban growth occurs in areas susceptible to multiple hazards, exposure to preexisting hazard risk increases. Additionally, urban development in the HKH has shaped landscapes in ways that further increase their susceptibility to hazards—destabilizing slopes in ways that predispose them to landsliding, blocking natural drainages in ways that intensify flooding, and disrupting ecosystem services that otherwise buffer against natural hazards (Ballesteros-Cánovas et al., 2020; Rimal et al., 2015; Tiwari and Joshi, 2020). Urban settlements in the HKH are notable for their largely unplanned and unregulated patterns of growth (Tiwari and Joshi, 2020). Despite the increasing intensity and frequency of compound hazards due to climate change, and growing risks tied to urbanization, mountainous areas have lagged behind lowland areas in meeting hazard mitigation goals (Ariza et al., 2013; Macchi, 2010; Wester et al., 2019). To mitigate hazard risk for small settlements distributed across wide areas, large-scale high-resolution assessments of multi-hazard susceptibility and exposure are critical.

The primary goal of this paper is to understand patterns of multi-hazard risk in the HKH region. To accomplish this, we assess spatial patterns of multi-hazard susceptibility, the environmental patterns determining single- and multi-hazard susceptibility, and population exposure to multi-hazard risk. We ask: What is the distribution of multi-hazard susceptibility in the HKH, what are its environmental characteristics, and how may overlapping hazards interact? What proportion of the HKH's population is exposed to multi-hazard risk and where are exposed populations located? Finally, how can the distribution of multi-hazard risk contribute to understanding the consequences of urbanization processes in the region?

Current methods for assessing single hazards have made meaningful contributions to our understanding of hazard risk, but are not easily adapted to evaluating the multi-hazard risk faced by urbanizing populations in the HKH. Multi-hazard risk or susceptibility is often assessed by assigning relative weights to susceptibility of each hazard, and combining weights from separate hazards into a single score, often via the Analytic Hierarchy Process (Aksha et al., 2020; Gautam et al., 2021; Skilodimou et al., 2019). Condensing susceptibility to multiple hazards into a composite score, however, conceals information essential to understanding multi-hazard risk such as the specific hazards present and their potential compounding and cascading interactions (Cutter, 2018; Kappes et al., 2012). The importance of understanding these interactions will increase as climate change increases the likelihood of compounding hazards (IPCC, 2021).

The prevalence of cascading and compounding multi-hazards defines the complex challenge of hazard mitigation in the HKH and intersects with the transboundary character of multi-hazard risk, as hazards span spatial scales from local to national and interact across national or other administrative boundaries. Studies in the HKH have evaluated multi-hazard susceptibility and risk at a number of scales and resolutions, but there are no large-scale high-resolution models of multi-hazard susceptibility in the region. The transboundary distribution of hazards and people is best represented by large-scale susceptibility modeling, yet the small-scale of mitigation strategies (e.g. in a particular settlement) requires high-resolution across the study area. Small-scale studies are usually delimited by a geographic or administrative boundary. A recent study described multi-hazard risk in Dharan, Nepal—an area of less than 200 km^2—by overlapping susceptibility maps for landslides, floods, and earthquakes with a map of social vulnerability to hazards (Aksha et al., 2020). While useful for understanding the variation in susceptibility within the district, the limited bounds of this study could not show the hazard susceptibility of Dharan relative its neighboring districts or national context, an important consideration where

populations are mobile and urbanization is an ongoing process (Aryal et al., 2018; Ehrlich et al., 2021). Conversely, the "mountain specific multi-hazard risk management framework" (MSMRMF) for assessing hazard susceptibility and capacity for risk mitigation is assessed at a much larger scale, including seven hazards across 12 Indian states with a total area over 500,000 km^2 (Sekhri et al., 2020). MSMRMF's unit of analysis isthe district , which range in area from hundreds to tens of thousands of square kilometers (Sekhri et al., 2020). Further, it only includes districts in India, while hazard risk and population movement in the HKH cross national borders (Aryal et al., 2018; Sekhri et al., 2020). While useful for planning at the national scale, MSMRMF cannot be used to inform smaller-scale mitigation efforts, especially when a susceptible area spans two administrative regions or an international border.

Some methodological issues in evaluating large-scale high-resolution multi-hazard susceptibility can be circumvented with the application of machine learning models trained and tested on remotely sensed environmental covariate data. Satellites orbit Earth regularly and collect comparable data across large areas. Passive remote sensing using solar reflectance can provide land cover and thermal information, while active remote sensing such as Synthetic Aperture Radar is sensitive to surface water and terrain (Pham-Duc et al., 2017). These satellite-derived covariates are efficient at monitoring hazard-forming environments consistently across large areas (Metternicht et al., 2005; Zhong et al., 2020). Machine learning techniques deal effectively with high dimensionality input data and can use the same ensemble of covariate data across multiple hazard catalogs without resorting to subjective weighting schemes. While machine learning models used in this way do not describe the physical processes causing hazard formation, their ability to describe the spatial distribution of hazard susceptibility with a high degree of accuracy has made their use increasingly common (Javidan et al., 2021; Pourghasemi et al., 2020).

Here, we use machine learning techniques, remotely sensed data, and catalogs of previous hazards to perform a multi-hazard assessment of the HKH. The HKH is prone to a large number of hazards, and this study focuses on three general, salient, and recurrent landscape hazards that may pose risks to urbanizing areas: floods, landslides, and wildfires. Floods are the most common and most destructive hazard type in the region (Wester et al., 2019); landslides in the HKH are common, and cursory analysis has shown residents' potential exposure to them may be high (Wester et al., 2019); wildfires are relatively less destructive, but climate change and urbanization pressure at the wildland-urban interface is expected to increase both their frequency and destructiveness in the future (Vilà-Vilardell et al., 2020). Earthquakes are a fourth salient hazard, but are not modeled explicitly; while seismic hazard varies across the region, the unpredictability of earthquakes and their long recurrence time lead us to assume earthquake susceptibility is generally high across the region (Stein et al., 2018). Climatic hazards (e.g. extreme heat, droughts) were excluded due both to data limitations and to focus the study on hazards in the landscape. While both economic assets and populations are exposed to hazards, this study focuses on population exposure as a more consistent basis for comparison as estimates of economic assets may vary across administrative boundaries, through time, and between hazard catalogs (Stäubli et al., 2018).

2. Study area

The HKH region is defined in different ways by different sets of stakeholders. This project used the bounds defined by the three-year NASA-funded study of which it is a part. This choice was motivated by existing relationships with collaborators in these areas and data limitations of parallel studies. The HKH study region (Fig. 1) covers a 608,100 km^2 arc across South Asia inclusive of the Indian states of Sikkim, Uttarakhand, and Arunachal Pradesh, the Indian union territories of Ladakh and Jammu and Kashmir, and the nations of Nepal and Bhutan. The region is between the latitudes of 25° 57′ 53″ N and 35° 30′ 5″ N, and the longitudes of 73° 45′ 47″ E and 97° 24′ 55″ E. Hereafter in this study, references to the Hindu Kush Himalaya (HKH) refer specifically to this study region. The entirety of the study region is seismically active due to the collision of the Indian Plate beneath the Eurasian Plate. Slippage between these plates creates elastic strain that, when released, leads to high-magnitude disastrous earthquakes (Bilham, 2001).

This dynamic geology, together with climate and topography, creates the conditions for the study region's dynamic hydrologic activity. The wider Himalayan region holds the headwaters of ten major rivers that supply freshwater to over 1.3 billion people, but can also lead to major rapid onset flooding (Molden et al., 2014). This same environment gives rise to floods and landslides, two major hazards in mountainous regions (Stäubli et al., 2018). The environmental conditions in the HKH lead to highly diverse plant communities, but the same vegetation also gives rise to destructive wildfires (Matin et al., 2017; Vilà-Vilardell et al., 2020).

The HKH is home to large and mobile human populations. In 2019, the wider Himalayan region was home to 240 million people, and the HKH study region home to 74 million (Rose et al., 2020). Population growth, however, is not uniform across the region, with major growth observed at elevations between 1000 and 3500 m AMSL and a declining population at elevations over 4500 m AMSL (Romeo et al., 2015). The population is moving and urbanizing, but infrastructural development and resource access are unevenly distributed. By national estimates, around one-quarter

Fig. 1. The HKH study region in context. Graphic underlay from NASA's Blue Marble seamless image mosaic (Vermote et al., 2007).

of the population is living in poverty, with those higher concentrations of impoverished people in more mountainous areas (Wester et al., 2019). Social vulnerability to hazards is higher for households experiencing poverty, as well as for women (Dilshad et al., 2019).

3. Data and methodology

Our aim is to assess multi-hazard risk over a large transboundary area. There are three criteria for the choice of data. First, we only used data with planetary coverage. Our transboundary approach requires data consistent across administrative boundaries and, of equal importance, we chose data suited to reproducibility and replicability of our methods in other mountainous regions. Second, we required the environmental covariate data to have temporal overlap with the hazard catalogs (which span 1998–2018) used for modeling. Hazard catalogs are central to our modeling approaching and their temporal range anchored the acceptable temporal range of environmental data. Finally, we selected environmental covariates representing a broad range of spheres of the environment—the lithosphere (e.g. soil type), the hydrosphere (e.g. proximity to water), the biosphere (e.g. land cover), and the atmosphere (e.g. air temperature)—that may contribute to predicting the distribution of hazards. To model multiple hazards from the same set of covariates, we aimed for wide coverage of environmental conditions.

All hazard instances were recorded as points and environmental covariates were continuous or categorical raster layers. Geographic patterns in hazard catalogs, environmental covariates, and population are summarized in Supplementary Fig. 1. Hazard catalogs are summarized in Table 1.

3.1. Hazard catalogs

3.1.1. Flood catalog

Flood catalog data were extracted from the Global Flood Inventory (GFI) compiled by Adhikari et al. (2010) covering global events from 1998 to 2008. These point data were collected from a number of sources, including existing flood catalogs—Emergency Disasters Database, Dartmouth Flood Observatory, ReliefWeb, and International Flood Network—as well as primary sources such as news reporting and public records. All events in the GFI were verified with news reports or announcements from government agencies (Adhikari et al., 2010). Catalog records include floods across eleven causes, including flooding due to dam outbursts, brief torrential rainfall, monsoonal rain, avalanches, or cyclones. The GFI contained 206 total flood instances within the study region. Within the study area, 87% of recorded flood events could not be reliably assigned a trigger, 6% of events can be attributed to monsoonal rain, and 3% to heavy rainfall.

3.1.2. Landslide catalogs

Two catalogs of landslide events were used as input data for the landslide susceptibility model: The Global Landslide Catalog (GLC) and the Global Fatal Landslide Database (GFLD) (Froude and Petley, 2018; Kirschbaum et al., 2010). The GLC focuses on precipitation-triggered landslides, and the catalog includes landslides, rock falls, avalanches, debris flows, and mudslides. In the HKH, 90% of events recorded in this catalog are characterized as landslides, 4% mudslides, and 3% as mudslides. The GFLD focuses on landslides that caused human casualties and is categorized by the landslide triggers. 82% of the events in the HKH recorded in the GFLD are triggered by rainfall, 9% from construction activity and illegal hillcutting, and 2% from earthquakes. These datasets were grouped and duplicate events removed to create a combined dataset with 2382 landslide events.

3.1.3. VIIRS fire archive

Wildfire incidence data were obtained from the VIIRS fire archive, a catalog of the VIIRS 375 m active fire detection product between 2012 and 2018 (Schroeder et al., 2014). Unlike the flood and landslide catalog data where every point represents the centroid of an entire hazard instance, each record in the VIIRS archive corresponds to the centroid of a single cell where an active fire was detected, not an entire wildfire. Due to this, there are two orders of magnitude more fire detections than landslide instances, and three more than flood instances. To prevent overfitting, a random 1% of the VIIRS archive data were used as input data for the wildfire susceptibility model.

3.2. Environmental covariates and population data

3.2.1. Digital elevation model

Topography contributes to hazard-forming environments and four topographic environmental covariates are included here: elevation, slope, aspect and flow accumulation. Topographic covariates affect, for example, the movement of water and stability of soil and are commonly included as factors in hazard models that assess flood and landslide susceptibility (Eini et al., 2020; Kornejady et al., 2017; Pourghasemi et al., 2019). We use a digital elevation model (DEM) from the Shuttle Radar Topography Mission (STRM) flown in the year 2000 (Rabus et al., 2003). These data were remotely sensed by radar interferometry with a resolution of 1 arc-second and the collection of data despite cloud cover, a persistent problem for remote sensing in the HKH. STRM data and their derivatives have been used in hazard assessments in the HKH for flooding (Aryal et al., 2020), forest fires (Banerjee, 2021), and landslides (Saleem et al., 2020). At high elevations, STRM may underestimate elevation by up to 10 m, and measures height above tree canopy in forested areas (Berthier et al., 2006; Sun et al., 2003). Slope is derived by determining the highest magnitude first derivative across each cell of the STRM DEM. Aspect denotes the downslope direction of each cell in degrees clockwise from true north. Flow accumulation is a hydrological parameter describing the number of cells upslope from any given cell—downslope cells will have higher flow accumulation values, while cells along a ridgeline will have flow accumulation values close to zero. Flow accumulation is related to the lateral movement of water through a watershed and can be a conditioning factor for fluvial flooding (Santos et al., 2019). Flow accumulation was calculated from the STRM DEM by the D-8 algorithm (O'Callaghan and Mark, 1984).

3.2.2. Climate data

Rainfall events can trigger flooding or landsliding (Aryal et al., 2018; Dahal and Hasegawa, 2008) and high rainfall during the monsoon season may raise the likelihood of wildfires when it is followed by hot dry fire seasons, as the growth of vegetation fed by monsoon rains

Table 1
Description of hazard catalogs for floods, landslides, and wildfires used for training and validation.

	Dataset	Number of records in study region	Time range
Floods	Digitized Global Flood Inventory[a]	206	1998–2008
Landslides	Global Fatal Landslide Database[b]	1018	2004–2017
	Global Landslide Catalog[c]	1416	2004–2016
Wildfires	VIIRS Fire Archive[d]	402,957	2012–2018

[a] Adhikari et al. (2010).
[b] Froude and Petley (2018).
[c] Kirschbaum et al. (2010).
[d] Schroeder et al. (2014).

becomes fuel as it dries in the hot weather that follows (Renard et al., 2012). We include the mean annual air temperature (°C) and annual precipitation amount (kg m^{-2}) data ranging 1981–2010 from CHELSA (Climatologies at High resolution for the Earth Land Surface Areas) v2.1, a climate dataset with global coverage at a 30 arcsecond resolution (Karger et al., 2017). Recent research in ecological niche modeling has indicated that quasi-mechanistical statistically downscaled climate data (i.e. CHELSA, Karger and Zimmermann, 2019) is preferable to interpolated data (i.e. WorldClim) in regions like the HKH where weather stations are scarce (Maria and Udo, 2017). CHELSA improves upon interpolated data in areas where orographic precipitation is a major factor (Maria and Udo, 2017; Karger et al., 2017).

3.2.3. Soil data

The properties of a soil affect its contribution to hazard-forming environments. For example, the shear strength of a soil is a property related to its propensity to slide, and a soil suborder's permeability affects how water moves through its matrix of or over its surface. In these models, FAO-UNESCO world soil suborder data were included as a categorical covariate at a resolution of 0.033 decimal degrees (FAO-UNESCO, 2005). This soil map is not remotely sensed, but is based on ground surveys and national data (FAO-UNESCO, 2005).

Soil moisture is related to the incidence of landslides and floods. High soil moisture lowers the shear strength of a soil, preconditioning slope failure and landsliding, and increases surface runoff, in turn increasing peak flow and flooding (Ray and Jacobs, 2007; Wasko and Nathan, 2019). Soil moisture data for the study region at a 15-km resolution was obtained from those published by the European Space Agency's Climate Change Initiative (Guevara et al., 2019). These data represent the average annual soil moisture values in volumetric water content (m^3/m^3) from 1991 to 2016.

3.2.4. Land cover

Land cover can contribute to hazard-forming environments and is commonly included in hazard susceptibility models (Aryal et al., 2020; Rimal et al., 2015; Vilà-Vilardell et al., 2020). We categorized cells in the study area into land cover classes using MDA's BaseVue 2013 data product. In the HKH, land cover is categorized by BaseVue as deciduous forest, evergreen forest, scrubland, grassland, barren, general agricultural, paddy agriculture, wetland, open water, ice or snow, high density urban, or medium density urban. BaseVue 2013 was selected for its global coverage, recent sampling, and 30 meter resolution. It is derived by an unsupervised algorithm from Landsat 8 imagery (MDA, 2014).

3.2.5. Distance to permanent water

Fluvial flooding occurs when a water body exceeds its capacity and floods its adjacent area, and thus has a direct relationship with the distance from a water body. Each cell in the study region was assigned a value describing its distance in decimal degrees to the nearest permanent water cell. Permanent water was defined as water that occurred more than 85% of the time. These data were derived from the Global Surface Water Explorer, a dataset that quantifies global surface water changes between 1984 and 2015 at 30-meter resolution (Pekel et al., 2016). These data are commonly cited in models of hydrologic hazards in the HKH (Mohanty and Maiti, 2021; Veh et al., 2019).

3.2.6. Population data

Gridded population data were used to determine populations at risk. LandScan data, the stated purpose of which is to estimate populations at risk, represents an ambient population count over a typical 24-hour period (Rose and Bright, 2014). LandScan uses a dasymetric method to disaggregate subnational census data into 30 meter cells (Rose and Bright, 2014). The ambient distribution of population differs from a residential distribution by the inclusion of local models of daily travel, cultural settlement patterns, land cover, and other spatial data (Dobson et al., 2000; Rose and Bright, 2014). The LandScan data were resampled to match the resolution of the multi-hazard map. The most recent LandScan dataset, collected in 2019, shows 74 million inhabitants are heterogeneously distributed across the study region, clustered in some areas and absent from others. No human habitation is recorded across 45% of the study region, and only 6% of the study region has an ambient population density of more than 500 persons-km^{-2}. The majority of the populated land area has a density of less than 50 persons-km^{-2}.

While LandScan is commonly used for hazard assessments, differences exist between its population estimates and those of other gridded population datasets (Smith et al., 2019). Here, the exposure assessment was repeated with the 2019 WorldPop dataset (Tatem, 2017) and the results compared.

3.2.7. Environmental covariate and population data resampling

Raster grids for all environmental data were resampled to 16 arcsecond (approximately 0.5 km) resolution. Continuous covariates were resampled using bilinear interpolation. Soil suborder was upsampled by assigning the value of the original larger cell to each new smaller cell within its bounds. Land cover was downsampled by assigning each new cell the most common value of the original cells within its bounds.

3.3. Susceptibility and exposure modeling

The process of generating the single and multi-hazard susceptibility models, and their use to determine the magnitude and distribution of exposure to multi-hazard risk, is outlined in Fig. 2.

3.3.1. Modeling hazard susceptibility

Individual hazard susceptibility models were created using a presence-only machine-learning method, Maximum entropy (Maxent) (Phillips et al., 2021). Maxent is freely available for noncommercial use as a multi-platform Java-based software and was originally built to model distributions of rare species. Maxent has become an established technique for modeling natural hazards such as floods, landslides, and wildfires (Eini et al., 2020; Kornejady et al., 2017; Pourghasemi et al., 2020; Renard et al., 2012). Maxent's presence-only approach is useful when hazard occurrences are rare and the terrain in the study region is not easily accessible, as it avoids the need to generate pseudo-absence data in areas where the actual non-occurrence of a hazard cannot be reliably known. Like other machine learning techniques, Maxent's output maps describe the hazard's distribution but not the mechanisms by which a hazard is triggered.

Maxent determines the distribution of hazards by finding the distribution with the highest degree of randomness within the constraints defined by the relationship between the input hazard instances and their environmental covariates. Outputs from the model are complementary log-log transformed, allowing the resulting values to be interpreted as the relative likelihood that the hazard will occur in that cell, i.e. the susceptibility of the cell to the hazard (Phillips et al., 2021). These transformed output values range from 0 to 1.

Maxent models were built from a set of ten environmental covariates for each of the three modeled hazards. The catalog data for each of the hazards was partitioned into 70% training and 30% test data. Catalog data in cells within the study area with a null value for any of the environmental covariates were excluded from the model.

3.3.2. Accuracy assessment and binary maps

The test data comprises 30% of the events in each hazard catalog included in the model and 10,000 absence samples randomly derived from the background area for each hazard. Area proportional sampling was used to evaluate the accuracy of binary mapping by using a default probability threshold of 0.5 (Chen et al., 2019; Stumpf and Kerle, 2011). With standard error of the overall accuracy at 1%, 787, 1005, and 1023 sample points are randomly drawn from the test data to evaluate the binary maps of floods, landslides and wildfires, respectively. In our

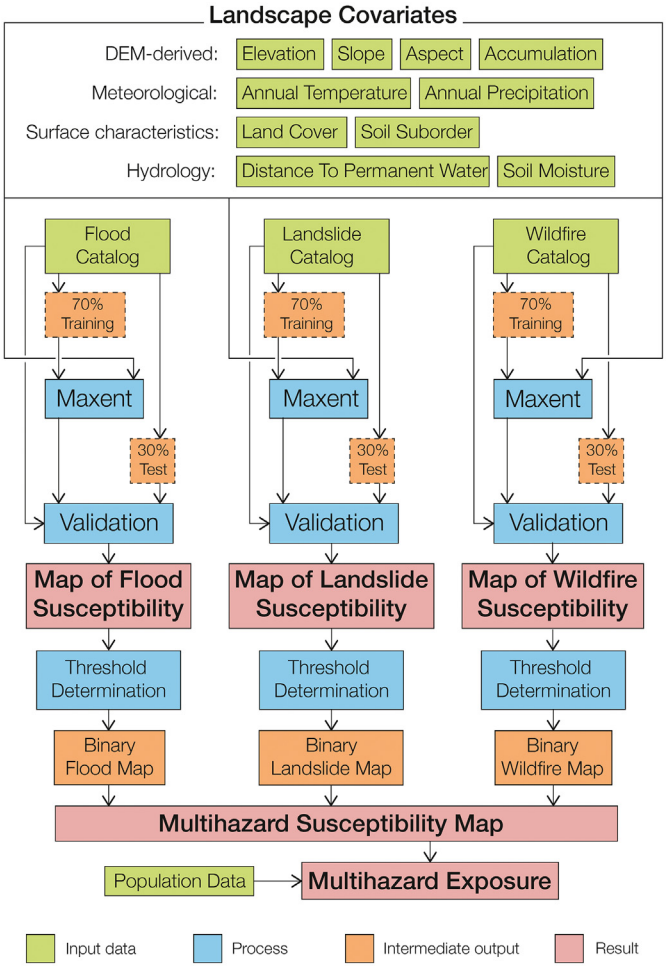

Fig. 2. Flowchart describing methodology for estimating single- and multi-hazard susceptibility and exposure.

preliminary analysis, we observed a higher incidence of type II than type I errors for all hazard models when using the 0.5 probability threshold, leading to the omission of real hazard events from the binary map.

Thus, we used an iterative resampling scheme to search for a threshold model value with the highest F1 score (i.e., harmonic mean of the model's precision and recall). The optimal threshold is defined at the highest mean F1 score of 99 iterations for each hazard model; cells above the threshold value were classed "high susceptibility" and cells below as "low susceptibility" for each hazard model. F1 scores ranged between 0 and 1, with a score of 1 representing a perfect model. The F1 scores and thresholds for each model are reported in Table 2. For each model, the Gini coefficient (2*AUC-1) was calculated to allow comparison with previously published studies.

3.3.3. Multicollinearity

To perform a test for multicollinearity, we built a linear regression model for each and calculated variance inflation factors (VIF) for each environmental covariate. Variance inflation factors between greater than 5 indicate that the covariate is correlated with at least one other covariate. Covariates with VIF greater than 5 are tested pairwise by Pearson's correlation coefficient to determine the nature of the correlation. As Maxent is robust against multicollinearity, collinear environmental covariates are not excluded from the model (Elith et al., 2011; Feng et al., 2019).

Table 2
Summary statistics for each of the three single-hazard models. Area under the receiver operating curve (AUC) is reported to show model performance against both training and test data. For each model, a threshold was determined by maximizing its associated F1 score.

	AUC_training	AUC_test	Threshold	F1
Floods	0.96	0.93	0.53	0.96
Landslides	0.92	0.91	0.42	0.93
Wildfires	0.86	0.86	0.45	0.92

3.3.4. Multi-hazard mapping

The thresholds determined for the flood, landslide, and wildfire models were used to create a binary map for each hazard, where all cells with output values equal to or above the threshold were assigned as highly susceptible cells and those below set to null. The binary maps were overlaid, and each cell was assigned a value indicating the set of hazards to which it was highly susceptible.

To determine exposure, the multi-hazard map was overlaid with the 2019 LandScan global population distribution data. To determine the population exposed to each category in the multi-hazard risk map, the LandScan population counts were summed for each hazard combination across every cell in the study region.

4. Results

4.1. Multi-hazard exposure

Our analysis shows nearly half (49%) of the region's population are exposed to multi-hazard risk and that high susceptibility to more than one hazard is geographically concentrated in one-third of the region's land area (Fig. 3). Conversely, 51% of the land area of the HKH has low susceptibility for all three hazards but only 19% of the 2019 population is present in this area (Fig. 3). The area highly susceptible to all three hazards simultaneously comprises only 9% of the study region's land area but was home to 21% of its 2019 population (Fig. 3). Trends in exposure held when we repeated out exposure assessment with the WorldPop data, which shows 20% of the population living in areas not highly susceptible to any hazard, 47% of the population in areas highly susceptible to multiple hazards, and 21% of the population within the 9% of the land area highly susceptible to all three modeled hazards.

The multi-hazard susceptibility map was assembled from three binary maps for each hazard. The proportion of the study region identified in the binary map as "highly susceptible" varied by hazard. The hazard with the largest highly susceptible area was wildfires, covering 39% of the study region. The area highly susceptible to landslides comprised 36% of the study area, and the area susceptible to flooding covered 13%.

4.2. Environmental covariates for multi-hazard susceptibility

The area of highest multi-hazard risk runs through the hill region in a band between the low-lying alluvial flats to the south and the mountainous areas to the north (Fig. 4). This band is generally highly susceptible to landslides and wildfires, with low-lying valleys and terraces also susceptible to flooding. The area highly susceptible to landslides, forest-fires and floods is south of the Great Himalayan mountains, running along the middle Himalayan ranges—sometimes referred to as the hill region and Sivalik hills—to the narrow belts of Bhabar and Tarai in the foothill region to the south.

Environmental covariates for cells highly susceptible to multiple hazards are distinct from those in cells highly susceptible to only a single modeled hazard or no hazard at all. Multi-hazard susceptibility is most common at elevations between 700 and 1800 m AMSL, while cells highly susceptible to only a single hazard vary widely in elevation, and low susceptibility cells are more common at higher elevations. Multi-hazard susceptibility is also clearly distinguished by the soil types where it is predicted. Over 60% of cells predicted to have high multi-hazard susceptibility are cells with udept soils, which are relatively young, high in organic content, and perennially moist. Conversely, udept soils cover less than 5% of cells highly susceptible to only a single

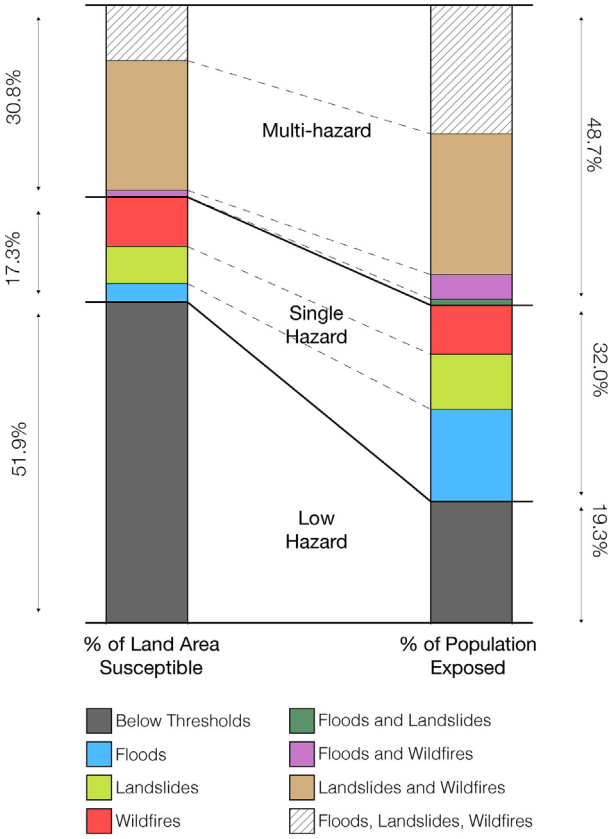

Fig. 3. Comparison of the proportion of land area susceptible to each hazard and hazard combination with the proportion of the population living in high susceptibility areas.

modeled hazard, and 1% of cells not highly susceptible to any modeled hazard. Cells predicted as highly susceptible to multiple modeled hazards have higher annual temperatures than the rest of the region, though this effect may be difficult to separate from the effect of elevation due to the collinearity between those covariates (described below). In summary, multi-hazard susceptibility is distributed across mid-elevation areas that are relatively hotter than upslope areas and marked by young wet soils high in organic content. These same areas have higher relative incidence of human settlement.

4.3. Single hazard susceptibility models and their environmental covariates

The Maxent model outputs were used to create three raster maps of the study region at 16 arc-second resolution illustrating the regional pattern of susceptibility to each hazard (Fig. 5). When the model outputs were validated against the reserved test data, the AUC values were 0.93, 0.91, and 0.86 for the models of floods, landslides and wildfires respectively. In the same order, Gini coefficients for these three models are 0.86, 0.82, and 0.72. In each model, VIF were less than 5 for all covariates with the exception of elevation and temperature, which had VIF > 10. Elevation and temperature are very strongly negatively correlated (PCC = −0.98) in the study region. As Maxent is robust against collinearity, neither elevation nor temperature is removed from the model.

The contributions of each environmental covariate to the hazard models are summarized in Fig. 6. Of the ten covariates evaluated across the models, annual precipitation amount, elevation, and soil suborder had significant contributions to all three models. Mean annual precipitation amount contributed 41%, 26%, and 61% to models of floods, landslides, and wildfires respectively. The mean annual precipitation amount for areas highly susceptible to floods, landslides, wildfires was 2.2×10^3 kg-m^{-2}-yr^{-1}, similar to mean precipitation across the region, though landslide-susceptible landscapes occur over wider spread of precipitation values than wildfires. Landscapes highly susceptible to flooding have slightly lower mean annual precipitation values ($\bar{x} = 2.1 \times 10^3$ kg-m^{-2}-yr^{-1}) than the other modeled hazards.

Elevation contributed 22%, 17%, and 21% to the models of floods, landslides, and wildfires respectively. Two-thirds of areas highly susceptible to floods were predicted below 1000 m AMSL, while wildfire and landslides predictions were clustered around respective mean elevations of 1200 and 1600 m AMSL. All three models underestimate susceptibility at very high elevations (above 3000 m AMSL) where less than 3% of any hazard catalog is recorded and there is low or no population. Soil suborder contributed 19%, 31%, and 7% to the models of floods, landslides, and wildfires respectively. Flood predictions were highest in valley bottoms with young and perennially moist soils in the udept soil suborder. Landslide and wildfire predictions were high on udept soils, but also on rocky orthent substrates.

Other covariates had significant contributions to only one of the models. Distance to permanent water had a contribution factor of 8% in the flood model, a signal that fluvial flooding occurs adjacent permanent waterways but the relative magnitude of its contribution suggests that flooding in areas farther from permanent water is also common. Slope had a contribution factor of 17% in the landslide model. Landslide predictions are very low for all slopes less than 4° and relatively evenly

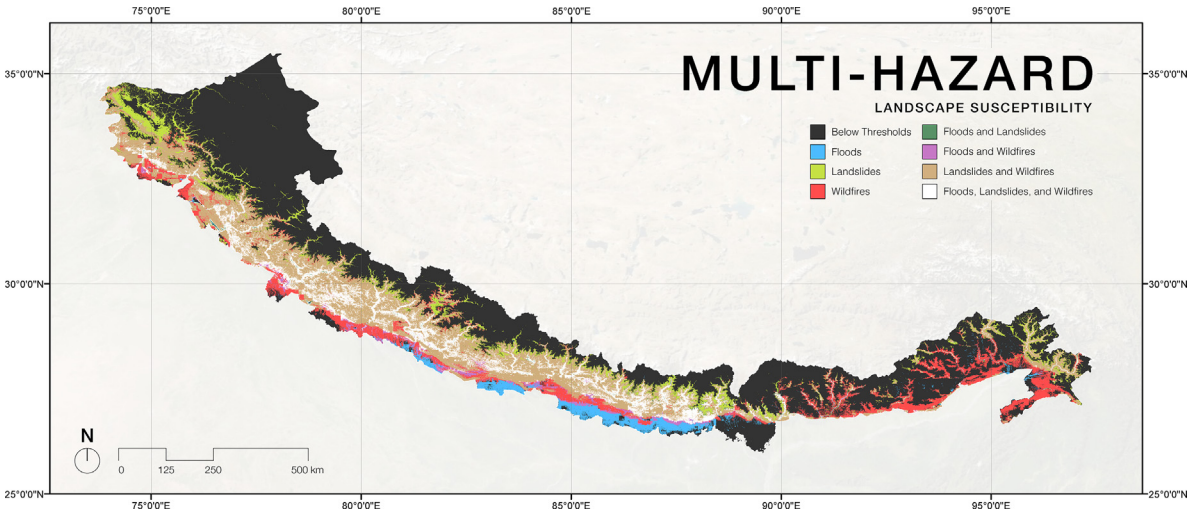

Fig. 4. Spatial distribution of multi-hazard susceptibility.

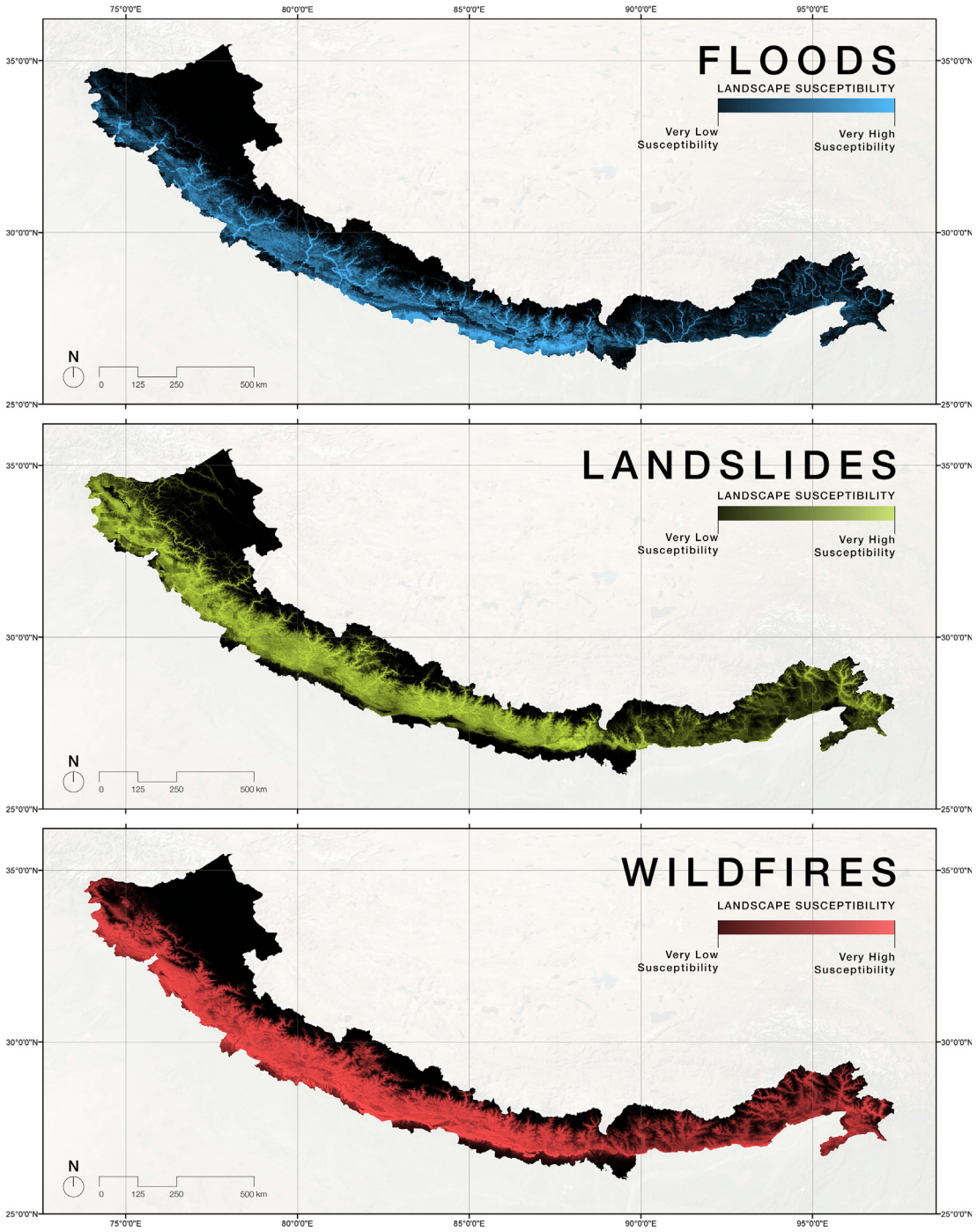

Fig. 5. Spatial distribution of flood, landslide, and wildfire susceptibility.

distributed across steeper slopes. Land cover had a contribution factor of 10% to the wildfire model; fire predictions are higher in areas with evergreen forest cover, but also notable in deciduous forests and scrublands. The remaining four environmental covariates—aspect, annual temperature, flow accumulation, and soil moisture—each contributed less than 5% to any single model.

5. Discussion

5.1. Multi-hazard susceptibility and exposure

Multi-hazard risk is the reality for nearly half (49%) of those who live in the HKH, a level of exposure disproportionate to the distribution of multi-hazard susceptibility. Contrasting this, only one-fifth of the population lives in the over 50% of the region with low susceptibility to all three modeled hazards. Machine learning models built from recent remotely sensed landscape data and hazard catalogs provide robust support for this conclusion. All three individual hazard models had Gini coefficients greater than 0.6, understood in the literature as a threshold for model accuracy (Pourghasemi et al., 2020). This finding of high exposure to multi-hazard risk has been borne out by multi-hazard studies in the HKH focused on smaller areas delimited by administrative boundaries, but the results here describe the transboundary distribution of both hazard susceptibility and human settlement (Aksha et al., 2020; Gautam et al., 2021; Mukherji et al., 2018; Zhang et al., 2017).

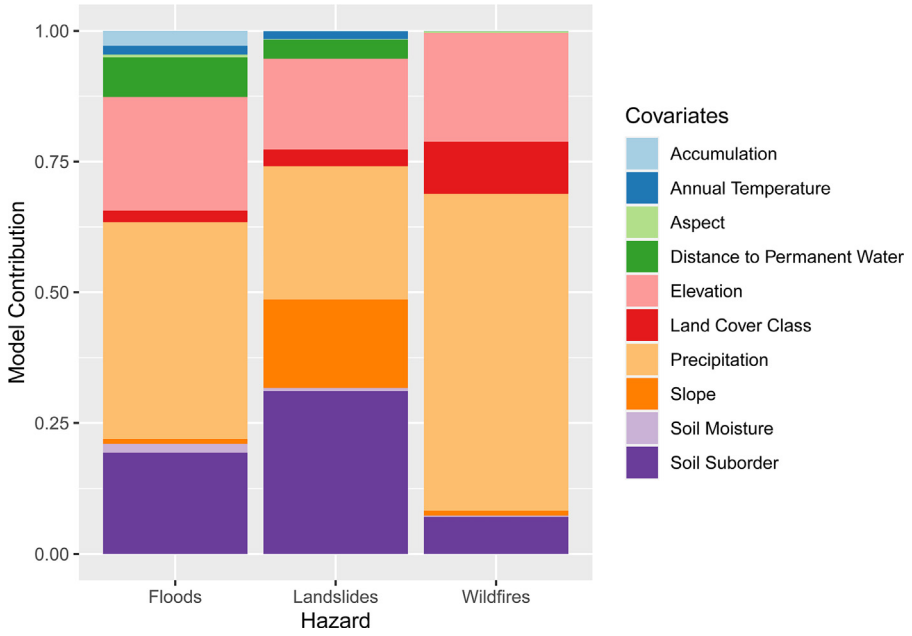

Fig. 6. Contributions of each covariate to the performance of each single-hazard model.

The spatial co-incidence between multi-hazard risk and human settlement relates to the landscape characteristics favorable to both. All three modeled hazards coincide in densely-populated valleys in the mid-elevation hill regions of the HKH. These valleys, which span national boundaries, are the major corridors for current urbanization in the region (IHCAP, 2017; Mukherji et al., 2018). The environmental characteristics favorable to settlement and agriculture—such as lower elevation, warmer temperatures, and soils with perennial moisture—are also contributors to multi-hazard susceptibility. At present, urban growth in less hazardous environments is less common, as settlement patterns in the HKH are tightly constrained by the availability of topography and climate suitable to current "ribbon sprawl" urbanization in the HKH, where urban growth in highly susceptible areas occurs along valley road corridors through agriculturally productive areas (Diksha and Kumar, 2017; IHCAP, 2017). Our study shows that these corridors are areas where multi-hazard risk exposure is high. Urbanization in these areas is driven by the availability of work, infrastructure, and access to education or healthcare (both public and private), not necessarily by the minimization of hazard risk (Aryal et al., 2020; Mukherji et al., 2018; Muzzini and Aparicio, 2013). Urbanization processes in the HKH and increasing exposure to multi-hazard risk while climate change increases the frequency and intensity of compound hazards related to climate (IPCC, 2021; Molden et al., 2014; Tiwari and Joshi, 2020).

The importance of social patterns in determining exposure also inflects how this study may be applicable to other mountainous areas. At first glance, this study's finding appears to contrast a multi-hazard assessment in Austria which showed that multi-hazard exposure of Austria's building stock in mountainous regions is very low; the wide difference in level of development between Austria and the HKH, however, allows us to understand this difference as aligned with our finding that exposure to multi-hazard risk is driven by social and economic processes, not necessarily overall incidence of multi-hazard susceptibility (Fuchs et al., 2015; UNDP, 2019).

In addition to clarifying the relationship between multi-hazard risk and urbanization processes, this study improves upon both small- and large-scale multi-hazard assessments in the HKH. Our results build upon small-scale studies that demonstrate exposure to multi-hazard risk is not driven primarily by hazard susceptibility but by social patterns (Dharan, 2015), while problematizing the conclusions of coarser large-scale assessments whose description of high multi-hazard exposure follows from an analysis showing high incidence of hazard-susceptible landscapes (Dilley et al., 2005; Sekhri et al., 2020).

5.2. Multi-hazard interaction, risk and mitigation

Since these hazards arise from landscape characteristics common to all three models, areas of high multi-hazard susceptibility can be determined by the overlap of multiple individual hazards (Kappes et al., 2010). Multi-hazard environments differ from single-hazard environments by the mechanistic connections between hazards, where one hazard cascades from or compounds the effects of another (Cutter, 2018). However, machine learning models describe the areas in which multi-hazard risk is distributed but are agnostic to the mechanisms that give rise to multi-hazards.

To complement the models of hazard distribution, a multi-hazard matrix is assembled to describe the interactions between hazards in the HKH (Fig. 7). Hazard interaction matrices identify the influence of one hazard on another (Kappes et al., 2010). The hazards are arranged on the matrix's right diagonal, and each cell describes the effect of the row hazard on the column hazard. Each cell is filled with a description of compounding or cascading interaction between the hazards found in the literature on hazards in the HKH. When they are recorded in a specific location, these interactions are located on a map of the region (Fig. 7).

The matrix records three kinds of hazard interaction: where hazards are directly linked, where their linkage is mediated by an environmental condition, or where their linkage is mediated by infrastructure or urban processes. In the first case, hazards interact directly. These interactions can happen over short time spans, like when flooding erodes unstable soils to cause landsliding, or longer ones, when dams formed by previous landsliding may be breached by runoff from heavy precipitation upstream (Bhambri et al., 2016; Gupta and Sah, 2008). The 2015 Gorkha earthquake, for instance, cascaded to cause 24,000 landslides (Roback et al., 2018). Earthquakes are also capable of triggering glacial lake outburst floods with potentially devastating effects (Meyer et al., 2006). In other cases, the effect of one hazard on another is mediated by changes to an environmental condition brought about by the primary hazard. For instance, wildfires can change the properties of some soil substrates, lowering the precipitation threshold at which a slope will fail and a landslide will form (Abbate et al., 2019; Hodgkins, 2013). Wildfires

Earthquakes (EQ)	Earthquake breaks dam to cause outburst flooding ① EQ → FL	Coseismic landsliding ② EQ → LS	Earthquake damage to energy infrastructure causes fire ③ EQ → WF
- FL → EQ	**Floods (FL)**	Flooding causes erosion that destabilizes slopes ④ FL → LS	- FL → WL
- LS → EQ	Landslide dam formation leads to landslide lake outburst flood ⑤ LS → FL	**Landslides (LS)**	Landslide damage to energy infrastructure causes fire ⑥ LS → WF
- WF → EQ	Fire lowers a soil's water storage capacity, increasing runoff volume ⑦ WF → FL	Post-fire soil destabilization increases landslide risk ⑧ WF → LS	**Wildfires (WF)**

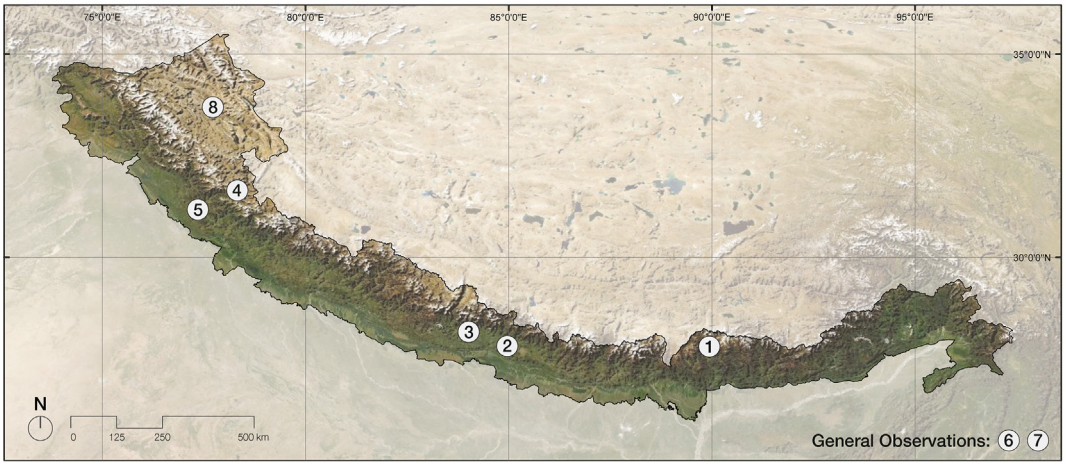

	Description	Study Location	Citation
①	Coupled flood and earthquake models show that an earthquake-trigged GLOF could flood 42% of infrastructure in a downstream village.	Eastern Lunana, Bhutan	Meyer et al., 2006
②	The 2015 Gorkha earthquake caused over 25,000 landslides with a total area of 87 square kilometers.	Gorkha, Nepal	Roback et al., 2018
③	In a multi-hazard assessment of land use transition, damage to petrol stations during earthquakes is considered the dominant fire hazard.	Pokhara Valley, Nepal	Rimal et al., 2015
④	In 2013, the breaching of Chorabari Lake caused erosion that led to landsliding that destroyed buildings, bridges, and a hydropower site.	Kedernath, Uttarakhand, India	Bhambri et al., 2016
⑤	In 2003, a landslide formed a dam blocking a tributary of the Spiti river; the failure of that dam in 2005 caused $155 USD in damage to infrastructure.	Kinnaur district, Himachal Pradesh, India	Gupta and Sah, 2008
⑥	Landslide damage to energy infrastructure may ignite wildfires.	*General observation*	OSCE, 2016
⑦	Wildfire can lower the water storage capacity of the landscape, leading to faster and deeper flash flooding,	*General observation*	Shakesby and Doerr, 2006
⑧	Forest fires are identified as a cause of landslides in the area because post-fire slopes tend to be less stable.	Leh Valley, Ladakh	Hodgkins, 2013

Fig. 7. Hazard interaction matrix illustrating possible relationships between hazards (above). The hazards are arranged on the matrix's right diagonal, and each cell describes the effect of the row hazard on the column hazard. When they are recorded in a specific location, these hazards are located on a map (center) and some recorded interactions are briefly described (below).

may also lower the soil's moisture holding capacity, increasing runoff and contributing to downslope flooding (Shakesby and Doerr, 2006). A third case is when the relationship between hazards is mediated by infrastructure or urban processes, such as when earthquake or landslides result in damage to energy infrastructure which in turn leads to fires (Hodgkins, 2013; OSCE, 2016), or when these hazards cause damage to a dam that leads to flash-flooding. The pairwise description of hazard interactions in the matrix illustrates linkages between hazards, but is nonexhaustive and does not preclude interaction between more than two hazards. While this matrix allows us to consider hazard linkages, the mechanisms for compounding or cascading hazards in the HKH is neither comprehensively described by this matrix nor

comprehensively understood. As climate change increases the incidence of complex hazards (IPCC, 2021), these hazard interactions may become increasingly definitive of hazard risk in the HKH and further study of them is warranted.

In multi-hazard environments like the HKH, accounting for the interaction between the hazards can avoid maladapted mitigation while suggesting synergistic strategies reducing risk. These synergistic strategies may consider, for instance, aspects of the environment related to multiple hazards. For example, this study shows soil character to be a major predictor of high susceptibility to floods, landslides, and wildfires and the hazard interaction matrix records multiple interactions related to soil (WF-FL, WF-LS, FL-LS). Erosion control measures for weak soils can synergistically mitigate against sudden landslides while also preventing the slow process of river siltation, which exacerbates downstream flooding (Tiwari, 2000). Conversely, fuel reduction to mitigate fire risk can increase erosion by removing root reinforcement and increasing sediment yields (Robichaud et al., 2010)—a maladaptive strategy that mitigates wildfire risk while amplifying flood and landslide risk by not accounting for common environmental covariates or interaction between hazards.

Multi-hazard risk crosses national boundaries and is present across spatial scales; to reduce these risks, mitigation measures addressing multi-hazard risk must also be transboundary and transscalar. Our study finds that exposure to multi-hazard risk is high, and its distribution does not follow administrative boundaries (Fig. 4). In the HKH, the transboundary distribution of multi-hazard susceptibility parallels transboundary patterns of human migration and settlement (Mukherji et al., 2018; Zhang et al., 2017). Further, administrative boundaries in the region are not fixed, a situation exemplified by the 2017 administrative restructuring in Nepal or the Government of India's 2019 partitioning of Jammu and Kashmir into two union territories. Administrative divisions (i.e. between scales of governance) may also hinder multi-hazard mitigation by assigning jurisdiction for different hazards to different agencies or levels of governance. Federalization in Nepal gave national authorities responsibility for wildfire management, but the onus for managing linked hazards, like floods or landslides, remains at the municipal scale. Collaborative governance approaches to address mismatches like this are emerging in the region, but are hampered by historical paradigms that focus on disaster response over risk reduction and by competition between administrative bodies or international NGOs (Russell et al., 2021; Vij et al., 2020). On smaller scales, many HKH residents in multi-hazard environments have detailed knowledge of multi-hazard processes, and their knowledge should be central to mitigation planning efforts (Gagné, 2019; Rieger, 2021). The distribution of hazards supports calls for coordination across boundaries while the character of hazard risks calls for coordination across scales—large-scale transboundary cooperation for disaster risk reduction has its counterpart in specific mitigation efforts, which often operate at household or municipal scales (ICIMOD, 2017; Klein et al., 2019; Vij et al., 2020).

5.3. Limitations and future research

While this study offers a robust assessment of multi-hazard susceptibility and exposure across the HKH, there are limitations to its method. This study gives a snapshot of multi-hazard susceptibility in a highly dynamic region. The static models in this study perform well in describing historical hazards but anthropogenic climate change and urbanization are rapidly reshaping the environment in the HKH, which in turn may reshape the distribution of future hazards (IHCAP, 2017; Mukherji et al., 2018; Wester et al., 2019). Specifically, climate change is expected to increase the incidence of compound hazards, further increasing multi-hazard risk in mountainous environments (IPCC, 2021). The performance of these models is driven by global datasets describing historical environmental processes and predictions of future patterns of multi-hazard susceptibility could use a parallel methodology to predict future hazard risk from projections of the region's future environmental conditions.

The second limitation is that translating our assessment of exposure into an assessment of risk will require additional data on differences in social vulnerability within populations (Rigg et al., 2016). To complement transboundary susceptibility models, fine-grained social and economic data can direct mitigation efforts toward the region's most vulnerable residents. Differences in sensitivity to disaster impacts or in the adaptive capacity of social groups may create significant differences in the vulnerability to hazards between population segments. Poverty, for instance, increases vulnerability, and this is an essential consideration because poverty may be a driver for settlement in high-risk areas (Tuladhar et al., 2015). While poorer residents will be more vulnerable to the coincidence of multiple hazards, gender disparities and social disparities mean that poor women and historically marginalized communities are especially vulnerable (Dilshad et al., 2019; Wester et al., 2019). Urbanizing areas are often home to poor and marginalized people—as well as elites—and additional social vulnerability data could elucidate the relationship between the distribution of multi-hazard risk and existing inequities (Mukherji et al., 2018).

A comprehensive multi-hazard assessment would describe every hazard to which a region is susceptible, but data limitations restrict this study to a subset of hazards present in the HKH. In addition to the three salient landscape hazards modeled here, and the high earthquake susceptibility throughout the region, avalanches, drought, and extreme heat are three other hazards identified as warranting transboundary assessments in the HKH (Wester et al., 2019). As spatialized transboundary catalogs of these hazards become available, or existing catalogs are expanded and resolved, this study's method could be expanded to include models of their distribution.

This study comes up against the limitations of hazard catalog and environmental covariate data. The resolution and size of the hazard catalogs prevents the reliable distinction between hazards in the same category but with different triggers, such as between fluvial and pluvial flooding or between rock fall and debris flow landsliding. This study focuses on building robust transboundary models, but larger and more comprehensive hazard catalogs could support the distinction between related hazard types in models using similar methods. Improved data may also allow future transboundary models to include environmental covariates more commonly utilized in small-scale studies (e.g. drainage networks in Aksha et al., 2020) at the transboundary scale. This study uses data describing the region's previous environment and hazards over a wide temporal range to construct a model highly capable of predicting recorded hazard incidence, but both hazards and the environment in the HKH are changing. In the future, additional data may allow temporal harmonization of recent environmental covariate data. Despite the data limitations of this study, it establishes that multi-hazard risk is, and will likely increasingly be, the reality for a large proportion of residents in the HKH despite the relatively low proportion landscape susceptible to multiple hazards.

6. Conclusions

This study establishes that the population in the HKH is concentrated in areas susceptible to multiple hazards and suggests that current patterns of human movement will continue to increase exposure to multi-hazards. Our findings are based on a suite of validated maps for three salient biophysical hazards (floods, landslides, wildfires) in the HKH, a map of multi-hazard susceptibility for the region, and an assessment of population exposure to multi-hazard risk. These maps illustrate that areas of high multi-hazard risk, typically warm low-altitude foothill areas with perennially moist soils, are also areas of with high levels of human settlements. If current trends continue, urbanization processes are likely increase exposure to multi-hazard risk while climate change increases the frequency and intensity of compounding hazards. Directing mitigation efforts in urbanizing areas toward multi-hazard

risk and hazard interactions, rather than single-hazard risk, can avoid maladaptation. Further research can expand our understanding of multi-hazard risk and its changing character in the dynamic HKH region.

Supplementary data to this article can be found online at https://doi.org/10.1016/j.scitotenv.2021.150039.

CRediT authorship contribution statement

Jack Rusk: Writing – original draft, Conceptualization, Methodology, Visualization, Writing – review & editing. **Amina Maharjan:** Writing – review & editing, Conceptualization. **Prakash Tiwari:** Writing – review & editing, Conceptualization. **Tzu-Hsin Karen Chen:** Writing – review & editing, Methodology, Validation. **Sara Shneiderman:** Writing – review & editing, Conceptualization. **Mark Turin:** Writing – review & editing, Conceptualization, Funding acquisition. **Karen C. Seto:** Writing – review & editing, Conceptualization, Supervision, Funding acquisition, Project administration.

Declaration of competing interest

The authors declare that they have no known competing financial interests or personal relationships that could have appeared to influence the work reported in this paper.

Acknowledgements

This research was funded by NASA LCLUC Grant NNX17AH98G. This study benefited from the insights and input offered by Meredith Reba, Aaron Tannenbaum, Emma Levin, Bhagwati Joshi, and the participants of the Himalaya Workshop at Yale in 2019, funded by the Edward J. and Dorothy Clarke Kempf Memorial Fund at Yale University.

References

Abbate, A., Longoni, L., Ivanov, V.I., Papini, M., 2019. Wildfire impacts on slope stability triggering in mountain areas. Geosciences 9, 417. https://doi.org/10.3390/geosciences9100417.

Adhikari, P., Hong, Y., Douglas, K.R., Kirschbaum, D.B., Gourley, J., Adler, R., Robert Brakenridge, G., 2010. A digitized global flood inventory (1998–2008): compilation and preliminary results. Nat. Hazards 55, 405–422. https://doi.org/10.1007/s11069-010-9537-2.

Aksha, S.K., Resler, L.M., Juran, L., Jr, L.W.C., 2020. A geospatial analysis of multi-hazard risk in Dharan, Nepal. Geomat. Nat. Hazards Risk 11, 88–111. https://doi.org/10.1080/19475705.2019.1710580.

Arias, P.A., Bellouin, N., Coppola, E., Jones, R.G., Krinner, G., Marotzke, J., Naik, V., Palmer, M.D., Plattner, G.-K., Rogelj, J., Rojas, M., Sillmann, J., Storelvmo, T., Thorne, P.W., Trewin, B., Rao, K.Achuta, Adhikary, B., Allan, R.P., Armour, K., Bala, G., Barimalala, R., Berger, S., Canadell, J.G., Cassou, C., Cherchi, A., Collins, W., Collins, W.D., Connors, S.L., Corti, S., Cruz, F., Dentener, F.J., Dereczynski, C., Luca, A.Di, Niang, A. Diongue, Doblas-Reyes, F.J., Dosio, A., Douville, H., Engelbrecht, F., Eyring, V., Fischer, E., Forster, P., Fox-Kemper, B., Fuglestvedt, J.S., Fyfe, J.C., Gillett, N.P., Goldfarb, L., Gorodetskaya, I., Gutierrez, J.M., Hamdi, R., Hawkins, E., Hewitt, H.T., Hope, P., Islam, A.S., Jones, C., Kaufman, D.S., Kopp, R.E., Kosaka, Y., Kossin, J., Krakovska, S., Lee, J.-Y., Li, J., Mauritsen, T., Maycock, T.K., Meinshausen, M., Min, S.-K., Monteiro, P.M.S., Ngo-Duc, T., Otto, F., Pinto, I., Pirani, A., Raghavan, K., Ranasinghe, R., Ruane, A.C., Ruiz, L., Sallée, J.-B., Samset, B.H., Sathyendranath, S., Seneviratne, S.I., Sörensson, A.A., Szopa, S., Takayabu, I., Treguier, A.-M., van den Hurk, B., Vautard, R., von Schuckmann, K., Zaehle, S., Zhang, X., Zickfeld, K., 2021. Technical summary. In: Masson-Delmotte, V., Zhai, P., Pirani, A., Connors, S.L., Péan, C., Berger, S., Caud, N., Chen, Y., Goldfarb, L., Gomis, M.I., Huang, M., Leitzell, K., Lonnoy, E., Matthews, J.B.R., Maycock, T.K., Waterfield, T., Yelekçi, O., Yu, R., Zhou, B. (Eds.), Climate Change 2021: The Physical Science Basis. Contribution of Working Group I to the Sixth Assessment Report of the Intergovernmental Panel on Climate Change. Cambridge University Press (In Press).

Ariza, C., Maselli, D., Kohler, T., 2013. Mountains: Our Life, Our Future Progress and Perspectives on Sustainable Mountain Development. 90. Swiss Agency Dev. Coop. Cent. Dev. Environ.

Aryal, D., Wang, L., Adhikari, T.R., Zhou, J., Li, X., Shrestha, M., Wang, Y., Chen, D., 2020. A model-based flood hazard mapping on the southern slope of Himalaya. Water 12, 540. https://doi.org/10.3390/w12020540.

Aryal, S., Cockfield, G., Maraseni, T.N., 2018. Globalisation and traditional social-ecological systems: understanding impacts of tourism and labour migration to the transhumance systems in the Himalayas. Environ. Dev. 25, 73–84. https://doi.org/10.1016/j.envdev.2017.09.001.

Ballesteros-Cánovas, J.A., Koul, T., Bashir, A., del Pozo, J.M.B., Allen, S., Guillet, S., Rashid, I., Alamgir, S.H., Shah, M., Bhat, M.S., Alam, A., Stoffel, M., 2020. Recent flood hazards in Kashmir put into context with millennium-long historical and tree-ring records. Sci. Total Environ. 722, 137875. https://doi.org/10.1016/j.scitotenv.2020.137875.

Banerjee, P., 2021. Maximum entropy-based forest fire likelihood mapping: analysing the trends, distribution, and drivers of forest fires in Sikkim Himalaya. Scand. J. For. Res. 36, 275–288.

Bera, A., Mukhopadhyay, B.P., Das, D., 2019. Landslide hazard zonation mapping using multi-criteria analysis with the help of GIS techniques: a case study from Eastern Himalayas, Namchi, South Sikkim. Nat. Hazards https://doi.org/10.1007/s11069-019-03580-w.

Berthier, E., Arnaud, Y., Vincent, C., Rémy, F., 2006. Biases of SRTM in high-mountain areas: implications for the monitoring of glacier volume changes. Geophys. Res. Lett. 33. https://doi.org/10.1029/2006GL025862.

Bhambri, R., Mehta, M., Dobhal, D.P., Gupta, A.K., Pratap, B., Kesarwani, K., Verma, A., 2016. Devastation in the Kedarnath (Mandakini) Valley, Garhwal Himalaya, during 16–17 June 2013: a remote sensing and ground-based assessment. Nat. Hazards 80, 1801–1822. https://doi.org/10.1007/s11069-015-2033-y.

Bilham, R., 2001. Himalayan seismic hazard. Science 293, 1442–1444. https://doi.org/10.1126/science.1062584.

Chen, T.-H.K., Prishchepov, A.V., Fensholt, R., Sabel, C.E., 2019. Detecting and monitoring long-term landslides in urbanized areas with nighttime light data and multi-seasonal landsat imagery across Taiwan from 1998 to 2017. Remote Sens. Environ. 225, 317–327. https://doi.org/10.1016/j.rse.2019.03.013.

Cutter, S.L., 2018. Compound, cascading, or complex disasters: what's in a name? Environ. Sci. Policy Sustain. Dev. 60, 16–25.

Dahal, R.K., Hasegawa, S., 2008. Representative rainfall thresholds for landslides in the Nepal Himalaya. Geomorphology 100, 429–443. https://doi.org/10.1016/j.geomorph.2008.01.014.

Diksha, Kumar, A., 2017. Analysing urban sprawl and land consumption patterns in major capital cities in the Himalayan region using geoinformatics. Appl. Geogr. 89, 112–123. https://doi.org/10.1016/j.apgeog.2017.10.010.

Dilley, M., Chen, R.S., Deichmann, U., Lerner-Lam, A.L., Arnold, M., 2005. Natural Disaster Hotspots: A Global Risk Analysis. The World Bank.

Dilshad, T., Mallick, D., Udas, P.B., Goodrich, C.G., Prakash, A., Gorti, G., Bhadwal, S., Anwar, M.Z., Khandekar, N., Hassan, S.M.T., Habib, N., Abbasi, S.S., Syed, Md.A., Rahman, A., 2019. Growing social vulnerability in the river basins: evidence from the Hindu Kush Himalaya (HKH) Region. Environ. Dev., Conceptualizing and Contextualizing Gendered Vulnerabilities to Climate Variability in the Hindu Kush Himalayan Region. 31, pp. 19–33. https://doi.org/10.1016/j.envdev.2018.12.004.

Dobson, J.E., Bright, E.A., Coleman, P.R., Durfee, R.C., Worley, B.A., 2000. LandScan: a global population database for estimating populations at risk. Photogramm. Eng. Remote Sens. 66, 849–857.

Ehrlich, D., Melchiorri, M., Capitani, C., 2021. Population trends and urbanisation in mountain ranges of the world. Land 10, 255. https://doi.org/10.3390/land10030255.

Eini, M., Kaboli, H.S., Rashidian, M., Hedayat, H., 2020. Hazard and vulnerability in urban flood risk mapping: machine learning techniques and considering the role of urban districts. Int. J. Disaster Risk Reduct. 50, 101687. https://doi.org/10.1016/j.ijdrr.2020.101687.

Elith, J., Phillips, S.J., Hastie, T., Dudík, M., Chee, Y.E., Yates, C.J., 2011. A statistical explanation of MaxEnt for ecologists. Divers. Distrib. 17, 43–57. https://doi.org/10.1111/j.1472-4642.2010.00725.x.

FAO-UNESCO, 2005. World Soil Suborder Map.

Feng, X., Park, D.S., Liang, Y., Pandey, R., Papes, M., 2019. Collinearity in ecological niche modeling: confusions and challenges. Ecol. Evol. 9, 10365–10376. https://doi.org/10.1002/ece3.5555.

Froude, M.J., Petley, D.N., 2018. Global fatal landslide occurrence from 2004 to 2016. Nat. Hazards Earth Syst. Sci. 18, 2161–2181.

Fuchs, S., Keiler, M., Zischg, A., 2015. A spatiotemporal multi-hazard exposure assessment based on property data. Nat. Hazards Earth Syst. Sci. 16.

Gagné, K., 2019. Waiting for the flood: technocratic time and impending disaster in the Himalayas. Disasters 43 (4), 840–866.

Gautam, D., Thapa, S., Pokhrel, S., Lamichhane, S., 2021. Local level multi-hazard zonation of Nepal. Geomat. Nat. Hazards Risk 12, 405–423. https://doi.org/10.1080/19475705.2021.1879941.

Guevara, M., Taufer, M., Vargas, R., 2019. Gap-free global annual soil moisture: 15km grids for 1991–2016. Earth Syst. Sci. Data Discuss., 1–35 https://doi.org/10.5194/essd-2019-191.

Gupta, V., Sah, M.P., 2008. Impact of the trans-Himalayan landslide lake outburst flood (LLOF) in the Satluj catchment, Himachal Pradesh, India. Nat. Hazards 45, 379–390. https://doi.org/10.1007/s11069-007-9174-6.

Hodgkins, S., 2013. Mass movement events in the Himalaya: the impact of landslides on Ladakh, India. Geol. Glob. Dev. 15.

ICIMOD, 2017. ICIMOD Strategy and Results Framework. Kathmandu, Nepal.

IHCAP, 2017. Urbanisation Challenges in the Himalayan Region in the Context of Climate Change Adaptation and Disaster Risk Mitigation.

IPCC, 2021. Summary for policymakers. In: Masson-Delmotte, V., Zhai, P., Pirani, A., Connors, S.L., Péan, C., Berger, S., Caud, N., Chen, Y., Goldfarb, L., Gomis, M.I., Huang, M., Leitzell, K., Lonnoy, E., Matthews, J.B.R., Maycock, T.K., Waterfield, T., Yelekçi, O., Yu, R., Zhou, B. (Eds.), Climate Change 2021: The Physical Science Basis. Contribution of Working Group I to the Sixth Assessment Report of the Intergovernmental Panel on Climate Change. Cambridge University Press (In Press).

Javidan, N., Kavian, A., Pourghasemi, H.R., Conoscenti, C., Jafarian, Z., Rodrigo-Comino, J., 2021. Evaluation of multi-hazard map produced using MaxEnt machine learning technique. Sci. Rep. 11, 6496. https://doi.org/10.1038/s41598-021-85862-7.

Kappes, M.S., Keiler, M., Glade, T., 2010. From single- to multi-hazard risk analyses: a concept addressing emerging challenges. In: Malet, J.-P., Glade, T., Casagli, N. (Eds.), Kappes, M.S.; Keiler, Margreth; Glade, Thomas (2010). From Single- to Multi-hazard Risk Analyses: A Concept Addressing Emerging Challenges. In: Malet, Jean-Philippe; Glade, Thomas; Casagli, Nicola (Eds.) Mountains Risks: Bringing Science to Society (International Conference) (pp. 351–356). Strassbourg: CERG Editions. Presented at the Mountains Risks: Bringing Science to Society (International Conference). CERG Editions, Strassbourg, pp. 351–356.

Kappes, M.S., Keiler, M., von Elverfeldt, K., Glade, T., 2012. Challenges of analyzing multi-hazard risk: a review. Nat. Hazards 64, 1925–1958. https://doi.org/10.1007/s11069-012-0294-2.

Karger, D.N., Conrad, O., Böhner, J., Kawohl, T., Kreft, H., Soria-Auza, R.W., Zimmermann, N.E., Linder, H.P., Kessler, M., 2017. Climatologies at high resolution for the earth's land surface areas. Sci. Data 4, 1–20.

Karger, D.N., Zimmermann, N.E., 2019. Climatologies at High Resolution for the Earth Land Surface Areas CHELSA V1. 2: Technical Specification. Swiss Fed. Res. Inst. WSL Switz.

Kirschbaum, D.B., Adler, R., Hong, Y., Hill, S., Lerner-Lam, A., 2010. A global landslide catalog for hazard applications: method, results, and limitations. Nat. Hazards 52, 561–575.

Klein, J.A., Tucker, C.M., Steger, C.E., Nolin, A., Reid, R., Hopping, K.A., Yeh, E.T., Pradhan, M.S., Taber, A., Molden, D., Ghate, R., Choudhury, D., Alcántara-Ayala, I., Lavorel, S., Müller, B., Grêt-Regamey, A., Boone, R.B., Bourgeron, P., Castellanos, E., Chen, X., Dong, S., Keiler, M., Seidl, R., Thorn, J., Yager, K., 2019. An integrated community and ecosystem-based approach to disaster risk reduction in mountain systems. Environ. Sci. Policy 94, 143–152. https://doi.org/10.1016/j.envsci.2018.12.034.

Kornejady, A., Ownegh, M., Bahremand, A., 2017. Landslide susceptibility assessment using maximum entropy model with two different data sampling methods. Catena 152, 144–162. https://doi.org/10.1016/j.catena.2017.01.010.

Macchi, M., 2010. Mountains of the World–Ecosystem Services in a Time of Global and Climate Change: Seizing Opportunities–Meeting Challenges. International Centre for Integrated Mountain Development (ICIMOD).

MacDonald, Dettwiler and Associates Ltd. (MDA), 2014. BaseVue 2013: Global Land Cover.

Maria, B., Udo, S., 2017. Why input matters: selection of climate data sets for modelling the potential distribution of a treeline species in the Himalayan region. Ecol. Model. 359, 92–102. https://doi.org/10.1016/j.ecolmodel.2017.05.021.

Matin, M.A., Chitale, V.S., Murthy, M.S., Uddin, K., Bajracharya, B., Pradhan, S., 2017. Understanding forest fire patterns and risk in Nepal using remote sensing, geographic information system and historical fire data. Int. J. Wildland Fire 26 (4), 276–286.

Metternicht, G., Hurni, L., Gogu, R., 2005. Remote sensing of landslides: an analysis of the potential contribution to geo-spatial systems for hazard assessment in mountainous environments. Remote Sens. Environ. 98, 284–303. https://doi.org/10.1016/j.rse.2005.08.004.

Meyer, M.C., Wiesmayr, G., Brauner, M., Häusler, H., Wangda, D., 2006. Active tectonics in Eastern Lunana (NW Bhutan): implications for the seismic and glacial hazard potential of the Bhutan Himalaya. Tectonics 25.

Mohanty, L.K., Maiti, S., 2021. Regional morphodynamics of supraglacial lakes in the Everest Himalaya. Sci. Total Environ. 751, 141586. https://doi.org/10.1016/j.scitotenv.2020.141586.

Molden, D., Sharma, E., Acharya, G., 2016. Lessons from Nepal's Gorkha earthquake 2015. Lessons Nepal's Earthq. Indian Himalayas Gangetic Plains, pp. 1–14.

Molden, D.J., Vaidya, R.A., Shrestha, A.B., Rasul, G., Shrestha, M.S., 2014. Water infrastructure for the Hindu Kush Himalayas. Int. J. Water Resour. Dev. 30, 60–77. https://doi.org/10.1080/07900627.2013.859044.

Mukherji, A., Scott, C., Molden, D., Maharjan, A., 2018. Megatrends in Hindu Kush Himalaya: climate change, urbanisation and migration and their implications for water, energy and food. In: Biswas, A.K., Tortajada, C., Rohner, P. (Eds.), Assessing Global Water Megatrends, Water Resources Development and Management. Springer, Singapore, pp. 125–146 https://doi.org/10.1007/978-981-10-6695-5_8.

Muzzini, E., Aparicio, G., 2013. Urban Growth and Spatial Transition in Nepal: An Initial Assessment. World Bank Publications.

O'Callaghan, J.F., Mark, D.M., 1984. The extraction of drainage networks from digital elevation data. Comput. Vis. Graph. Image Process. 28, 323–344.

OSCE, 2016. Protecting Electricity Networks from Natural Hazards.

Pangali Sharma, T.P., Zhang, J., Koju, U.A., Zhang, S., Bai, Y., Suwal, M.K., 2019. Review of flood disaster studies in Nepal: a remote sensing perspective. Int. J. Disaster Risk Reduct. 34, 18–27. https://doi.org/10.1016/j.ijdrr.2018.11.022.

Pekel, J.-F., Cottam, A., Gorelick, N., Belward, A.S., 2016. High-resolution mapping of global surface water and its long-term changes. Nature 540, 418–422. https://doi.org/10.1038/nature20584.

Pham-Duc, B., Prigent, C., Aires, F., 2017. Surface water monitoring within Cambodia and the Vietnamese Mekong Delta over a year, with Sentinel-1 SAR observations. Water 9, 366. https://doi.org/10.3390/w9060366.

Phillips, Steven J., Dudík, Miroslav, Schapire, Robert E., 2021. Maxent software for modeling species niches and distributions (Version 3.4.1).Available from url: http://biodiversityinformatics.amnh.org/open_source/maxent/ (Accessed on 2021-07-25).

Pourghasemi, H.R., Gayen, A., Panahi, M., Rezaie, F., Blaschke, T., 2019. Multi-hazard probability assessment and mapping in Iran. Sci. Total Environ. 692, 556–571.

Pourghasemi, H.R., Kariminejad, N., Amiri, M., Edalat, M., Zarafshar, M., Blaschke, T., Cerda, A., 2020. Assessing and mapping multi-hazard risk susceptibility using a machine learning technique. Sci. Rep. 10, 3203. https://doi.org/10.1038/s41598-020-60191-3.

Rabus, B., Eineder, M., Roth, A., Bamler, R., 2003. The shuttle radar topography mission—a new class of digital elevation models acquired by spaceborne radar. ISPRS J. Photogramm. Remote Sens. 57, 241–262.

Ray, R.L., Jacobs, J.M., 2007. Relationships among remotely sensed soil moisture, precipitation and landslide events. Nat. Hazards 43, 211–222. https://doi.org/10.1007/s11069-006-9095-9.

Renard, Q., Pélissier, R., Ramesh, B.R., Kodandapani, N., 2012. Environmental susceptibility model for predicting forest fire occurrence in the Western Ghats of India. Int. J. Wildland Fire 21, 368. https://doi.org/10.1071/WF10109.

Rieger, K., 2021. Multi-hazards, displaced people's vulnerability and resettlement: Post-earthquake experiences from Rasuwa district in Nepal and their connections to policy loopholes and reconstruction practices. Prog. Disaster Sci. 11 p.100187.

Rigg, J., Oven, K.J., Basyal, G.K., Lamichhane, R., 2016. Between a rock and a hard place: vulnerability and precarity in rural Nepal. Geoforum 76, 63–74. https://doi.org/10.1016/j.geoforum.2016.08.014.

Rimal, B., Baral, H., Stork, N., Paudyal, K., Rijal, S., 2015. Growing city and rapid land use transition: assessing multiple hazards and risks in the Pokhara Valley, Nepal. Land 4, 957–978. https://doi.org/10.3390/land4040957.

Roback, K., Clark, M.K., West, A.J., Zekkos, D., Li, G., Gallen, S.F., Chamlagain, D., Godt, J.W., 2018. The size, distribution, and mobility of landslides caused by the 2015 Mw7.8 Gorkha earthquake, Nepal. Geomorphology 301, 121–138. https://doi.org/10.1016/j.geomorph.2017.01.030.

Robichaud, P.R., MacDonald, L.H., Foltz, R.B., 2010. Fuel management and erosion. Elliot William J Mill. Ina Sue Audin Lisa Eds Cumul. Watershed Eff. Fuel Manag. West. U. S. Gen Tech Rep RMRS-GTR-231 Fort Collins CO US Dep. Agric. For. Serv. Rocky Mt. Res. Stn. P 79–100 231, 79–100.

Romeo, R., Vita, A., Testolin, R., Hofer, T., 2015. Mapping the Vulnerability of Mountain Peoples to Food Insecurity. FAO, Rome.

Rose, A.N., Bright, E., 2014. The LandScan Global Population Distribution Project: Current State of the Art and Prospective Innovation. Oak Ridge National Laboratory, Oak Ridge, TN.

Rose, A.N., McKee, J.J., Sims, K.M., Bright, E.A., Reith, A.E., Urban, M.L., 2020. LandScan 2019.

Russell, C., Clark, J., Hannah, D., Sugden, F., 2021. Towards a collaborative governance regime for disaster risk reduction: exploring scalar narratives of institutional change in Nepal. Appl. Geogr. 134, 102516. https://doi.org/10.1016/j.apgeog.2021.102516.

Saleem, J., Ahmad, S.S., Butt, A., 2020. Hazard risk assessment of landslide-prone sub-Himalayan region by employing geospatial modeling approach. Nat. Hazards 102, 1497–1514. https://doi.org/10.1007/s11069-020-03980-3.

Santos, P.P., Reis, E., Pereira, S., Santos, M., 2019. A flood susceptibility model at the national scale based on multicriteria analysis. Sci. Total Environ. 667, 325–337. https://doi.org/10.1016/j.scitotenv.2019.02.328.

Schroeder, W., Oliva, P., Giglio, L., Csiszar, I.A., 2014. The new VIIRS 375 m active fire detection data product: algorithm description and initial assessment. Remote Sens. Environ. 143, 85–96.

Sekhri, S., Kumar, P., Fürst, C., Pandey, R., 2020. Mountain specific multi-hazard risk management framework (MSMRMF): assessment and mitigation of multi-hazard and climate change risk in the Indian Himalayan Region. Ecol. Indic. 118, 106700. https://doi.org/10.1016/j.ecolind.2020.106700.

Shakesby, R.A., Doerr, S.H., 2006. Wildfire as a hydrological and geomorphological agent. Earth-Sci. Rev. 74, 269–307. https://doi.org/10.1016/j.earscirev.2005.10.006.

Shrestha, A.B., Steiner, J., Nepal, S., Maharjan, S.B., Jackson, M., Rasul, G., Bajracharya, B., 2021. Understanding the Chamoli Flood: Cause, Process, Impacts, and Context of Rapid Infrastructure Development.

Skilodimou, H.D., Bathrellos, G.D., Chousianitis, K., Youssef, A.M., Pradhan, B., 2019. Multi-hazard assessment modeling via multi-criteria analysis and GIS: a case study. Environ. Earth Sci. 78, 47.

Smith, A., Bates, P.D., Wing, O., Sampson, C., Quinn, N., Neal, J., 2019. New estimates of flood exposure in developing countries using high-resolution population data. Nat. Commun. 10, 1814. https://doi.org/10.1038/s41467-019-09282-y.

Stäubli, A., Nussbaumer, S.U., Allen, S.K., Huggel, C., Arguello, M., Costa, F., Hergarten, C., Martínez, R., Soto, J., Vargas, R., 2018. Analysis of weather-and climate-related disasters in mountain regions using different disaster databases. Climate Change, Extreme Events and Disaster Risk Reduction. Springer, pp. 17–41.

Stein, S., Brooks, E.M., Spencer, B.D., Liu, M., 2018. Should all of Nepal be treated as having the same earthquake hazard? In: Kruhl, J.H., Adhikari, R., Dorka, U.E. (Eds.), Living Under the Threat of Earthquakes, Springer Natural Hazards. Springer International Publishing, pp. 27–44

Stumpf, A., Kerle, N., 2011. Object-oriented mapping of landslides using random forests. Remote Sens. Environ. 115, 2564–2577. https://doi.org/10.1016/j.rse.2011.05.013.

Sun, G., Ranson, K.J., Kharuk, V.I., Kovacs, K., 2003. Validation of surface height from shuttle radar topography mission using shuttle laser altimeter. Remote Sens. Environ. 88, 401–411. https://doi.org/10.1016/j.rse.2003.09.001.

Tatem, A.J., 2017. WorldPop, open data for spatial demography. Sci. Data 4, 1–4.

Tiwari, P.C., 2000. Land-use changes in Himalaya and their impact on the plains ecosystem: need for sustainable land use. Land Use Policy 17, 101–111. https://doi.org/10.1016/S0264-8377(00)00002-8.

Tiwari, P.C., Joshi, B., 2020. Challenges of urban growth in Himalaya with reference to climate change and disaster risk mitigation: a case of Nainital Town in Kumaon Middle Himalaya, India. In: Dimri, A.P., Bookhagen, B., Stoffel, M., Yasunari, T. (Eds.), Himalayan Weather and Climate and Their Impact on the Environment. Springer International Publishing, Cham, pp. 473–491 https://doi.org/10.1007/978-3-030-29684-1_23.

Tiwari, P.C., Tiwari, A., Joshi, B., 2018. Urban growth in Himalaya: understanding the process and options for sustainable development. J. Urban Reg. Stud. Contemp. India 4, 15–27.

Tuladhar, G., Yatabe, R., Dahal, R.K., Bhandary, N.P., 2015. Disaster risk reduction knowledge of local people in Nepal. Geoenviron. Disasters 2, 5. https://doi.org/10.1186/s40677-014-0011-4.

UNCED, 1992. Agenda 21: the Earth summit strategy to save our planet. Presented at the Results of the World Conference on Environment and Development: Agenda 21. United Nations, New York.
UNDP, 2019. Human Development Report 2019. Beyond Income, Beyond Averages, Beyond Today: Inequalities in Human Development in the 21st Century. United Nations Development Programme, New York.
UNISDR, 2015. The Economic and Human Impact of Disasters in the Last 10 Years. United Nations International Strategy for Disaster Reduction, Geneva, Switzerland.
Veh, G., Korup, O., von Specht, S., Roessner, S., Walz, A., 2019. Unchanged frequency of moraine-dammed glacial lake outburst floods in the Himalaya. Nat. Clim. Chang. 9, 379–383. https://doi.org/10.1038/s41558-019-0437-5.
Vermote, E., Saleous, N., Simmon, R., Herring, D., 2007. The Blue Marble Next Generation - A True Color Earth Dataset Including Seasonal Dynamics From MODIS.
Vilà-Vilardell, L., Keeton, W.S., Thom, D., Gyeltshen, C., Tshering, K., Gratzer, G., 2020. Climate change effects on wildfire hazards in the wildland-urban-interface – blue pine forests of Bhutan. For. Ecol. Manag. 461, 117927. https://doi.org/10.1016/j.foreco.2020.117927.
Vij, S., Russell, C., Clark, J., Parajuli, B.P., Shakya, P., Dewulf, A., 2020. Evolving disaster governance paradigms in Nepal. Int. J. Disaster Risk Reduction 50, 101911. https://doi.org/10.1016/j.ijdrr.2020.101911.
Wasko, C., Nathan, R., 2019. Influence of changes in rainfall and soil moisture on trends in flooding. J. Hydrol. 575, 432–441. https://doi.org/10.1016/j.jhydrol.2019.05.054.
Wester, P., Mishra, A., Mukherji, A., Shrestha, A.B. (Eds.), 2019. The Hindu Kush Himalaya Assessment: Mountains, Climate Change, Sustainability and People. Springer International Publishing, Cham https://doi.org/10.1007/978-3-319-92288-1.
Zhang, J., Regmi, A.D., Liu, R., Khanal, N.R., Schenato, L., Gurung, D.R., Wahid, S., 2017. Landslides inventory and trans-boundary risk management in Koshi River Basin, Himalaya. In: Li, A., Deng, W., Zhao, W. (Eds.), Land Cover Change and Its Eco-environmental Responses in Nepal, Springer Geography. Springer, Singapore, pp. 409–426 https://doi.org/10.1007/978-981-10-2890-8_18.
Zhong, C., Liu, Y., Gao, P., Chen, W., Li, H., Hou, Y., Nuremanguli, T., Ma, H., 2020. Landslide mapping with remote sensing: challenges and opportunities. Int. J. Remote Sens. 41, 1555–1581. https://doi.org/10.1080/01431161.2019.1672904.
Zimmermann, M., Keiler, M., 2015. International frameworks for disaster risk reduction: useful guidance for sustainable mountain development? Mt. Res. Dev. 35, 195–202.